Superconducting hydroformed niobium sputter coated copper cavities at 1.5 GHz

Ph. Bernard, D. Bloess, E. Chiaveri, C. Hauviller, T. Schiller, M. Taufer and W. Weingarten
CERN - European Organisation for Nuclear Research
CH–1211 Geneva 23 (Switzerland)

P. Bosland
CEN Saclay
F-91191 Gif-sur-Yvette Cedex (France)

A. Caruette, M. Fouaidy and T. Junquera
Institut de Physique Nucléaire
F-91406 Orsay Cedex (France)

Abstract

We report on the fabrication and testing of a series of monocell and pentacell superconducting 1500 MHz accelerating cavities, produced by hydroforming from a copper tube and coated by a thin Nb layer. By an improved and cleaner assembling of the magnetron cathode the stepwise Q degradation observed previously could be reliably suppressed. A temperature scanning system in superfluid helium which maps the RF losses is operational as diagnostic tool. Accelerating gradients of 15 MV/m at a Q-value of about 10^9 could be reproducibly obtained.

1. INTRODUCTION

Our work, which we started in 1990, was motivated by the necessity to obtain more insight into the RF performance of niobium sputter coated (NbCu) cavities for LEP. We chose 1500 MHz cavities because they allow a faster turnover compared to lower frequencies and a broader understanding of frequency dependent phenomena as, for example, the surface resistance. Two years ago, at the previous Workshop on RF Superconductivity, we reported for the first time on such cavities [1]. We proved, that in a monocell cavity accelerating gradients of about 15 MV/m at Q-values at 10^9 could be obtained. However, most of our monocell cavities were plagued by a stepwise degradation of the Q-value with the gradient ("Q-switches"). In a later paper [2], we investigated one of the basic features of NbCu cavities, their reaction to DC and RF magnetic fields. They exhibit a weak dependence of Q-value on a DC but a stronger one on an RF magnetic field, compared to conventional niobium sheet metal cavities. These investigations were motivated mainly by the wish to get a better understanding of the results from the series fabrication of NbCu cavities for LEP [3].
Another motivation, triggered by the workshops on a superconducting (SC) 1 TeV linear collider (TESLA), was the need for low cost, high Q and high gradient accelerating structures. The figures agreed upon are less than 50 k$/m including the cryostat and ancillaries [4], or 10 k$/m for the cavity alone [5] as fabrication costs, and a Q-value of $5 \cdot 10^9$ at 25 MV/m and 2 K. The technology available at CERN (hydroforming of Cu cavities) and Saclay (sputter coating equipment for 1500 MHz cavities) seemed to us a promising way to go.
Our effort, therefore, was directed towards an improvement of the diagnostic system, the elimination of "Q-switches", and the fabrication of multicell structures. This is what we will report upon.

2. CAVITY PRODUCTION

2.1 Hydroforming

The principle of hydroforming is to push the part against a rigid die by applying a large pressure through a liquid or a polymer [6]. This method has the advantage of producing monolithic pieces and therefore suppressing the need for welding, particularly in critical regions. Although the tooling is expensive, reproducible parts can be obtained in a straightforward way and at a very low cost in series production.

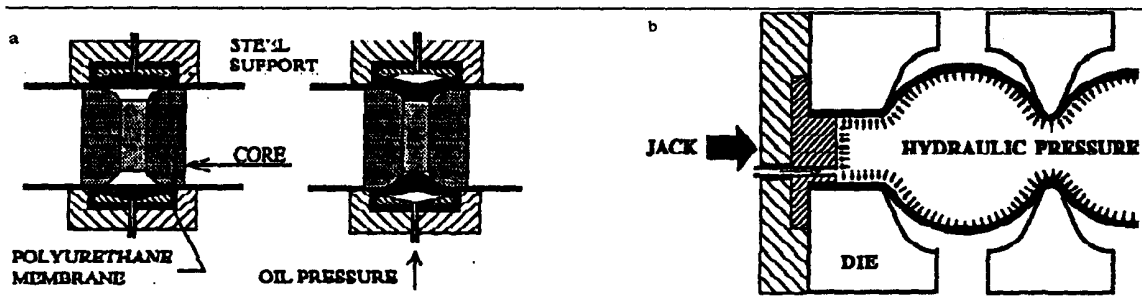

Fig. 1. Working steps of hydroforming pentacell cavities: a) Swaging and b) expansion step.

Cavities are produced from an OFE (Oxygen Free Electrolytic) copper tube, which has to withstand very large deformations, typically up to about 200%. Since the ultimate elongation of annealed copper is only of the order of 50%, the process must be multistage, including preliminary swaging (only for multicell, Fig. 1.a, and several expansions in a multi-part die, Fig. 1.b, with intermediate annealing at 600 °C for 1 hour).
The main nominal dimensions of a multicell cavity are:

Initial tube:	
Internal diameter	80mm
Thickness	2.5mm
Cavity:	
Minimum internal diameter (d)	70mm
Maximum internal diameter (D)	181.4mm
D/d	2.59
Minimum thickness	1.19mm
Dispersion of π-mode frequencies (pentacell cavities)	±450 kHz $\sim\pm 3\cdot 10^{-4}$

2.2 Chemical polishing

The hydroforming being completed, the last step of cavity fabrication is the welding of the cavity proper by electron beam to a copper tube, to which the Conflat flanges have been brazed before. The sequence of processing is the following: degreasing, passivation (chlorhydric and chromic acid), chemical polishing in a closed circuit with different fluids (sulfamic acid depassivation; chemical polishing solution: 5 g/l sulfamic acid H_3NO_3S, 5 % by volume hydrogen peroxide H_2O_2, 5 % by volume n-butanol $C_4H_{10}O$, 1 g/l ammonium citrate $C_6H_{14}N_2O_7$; sulfamic acid rinsing; water rinsing), assembling of upper and lower covers with pumping valve, rinsing with high pressure water and ethanol, drying by pumping, assembling of antennae to the covers, evacuating and venting with dry and filtered nitrogen. Then the cavity will be shipped to CEN Saclay for coating.

2.3 High pressure water rinsing

The rinsing with high pressure water [1] is a critical step in the whole procedure as it assures the cleanliness of the copper surface before coating. The water leaves a 0.04 µm membrane filter at the point of use under a pressure of 100 bar. The quality of the water entering and leaving the cavity is monitored. The resistivity of the input water is 18 MΩcm. The total organic carbon, as measured with a Shimadzu TOC analyser, and the non-volatile residues, as measured with a TSI Nonvolatile Residue Monitor are below 100 ppb. The rinsing is performed with a mass flow of 12 l/min (determined by 6 nozzles with 0.8 mm diameter each along the rod) and continues until the resistivity of the water at the cavity drain approaches that of the input water (well above 10 MΩcm). The rinsing is terminated (after 35 minutes for a monocell cavity) with a spray of high purity filtered ethanol in order to reduce oxidation of the copper.

2.4 Sputter coating

The films were prepared by DC magnetron sputtering using a cylindrical cathode. A new apparatus was developed in order to reduce dust contamination of the cavity walls before deposition (Fig. 2).

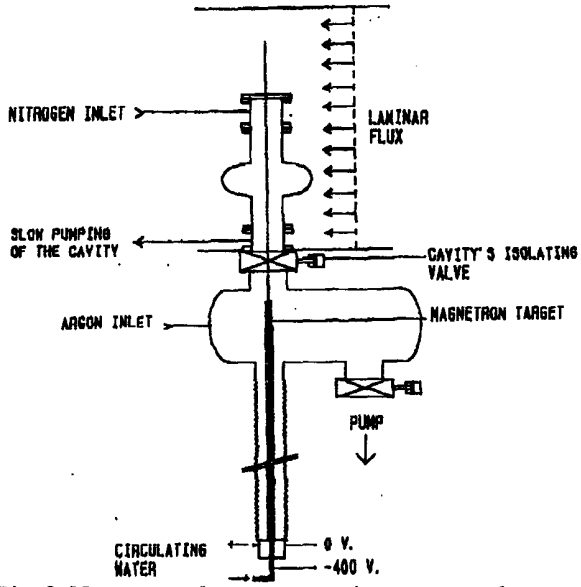

Fig. 2: New set-up for sputter coating mono- and pentacell cavities as well as samples in a dedicated sample chamber.

The cathode, made of high purity Nb (RRR = 250) is 10 cm long, 2 cm in diameter with 2 mm wall thickness. Permanent magnets, cooled by water flow, generate a 20 mT magnetic field parallel to the cathode surface. This cathode fixed to a bellows at the lower part of the set-up can be moved vertically into the cavity (or the sample chamber) situated at the top. A 100 mm diameter valve isolates the cavity from the bottom and allows separate pumping of the cavity or the lower part of the set-up. The sputtering facility is equipped with a cryopump (1500 l/s), a turbomolecular pump (50 l/s), and a primary pump. This second turbomolecular pump has two functions, the preliminary pumping of the set-up and the slow pumping of the cavities as described later. High purity (99.9995 %) Ar gas flow is regulated with a mass flow meter.
Nb samples on SiO_2 substrates were produced in a vacuum chamber placed on top of the sputtering equipment at the cavity's position. The critical temperature T_c and the RRR of the Nb films were measured (by four points resistive method). T_c values are 9.4 K with $\Delta T_c < 0.1$ K for Nb films deposited under the same conditions as for cavities. The overall RRR values of these films increase with their thickness (Fig. 3), irrespective of the position of the samples at the cavity

cell equator or at the iris. Similar results were presented in ref. 6.

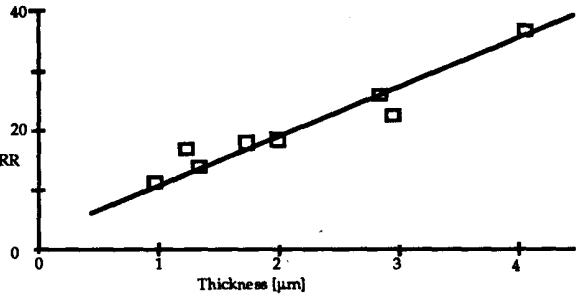

Fig. 3: RRR values of Nb films deposited on SiO_2 substrates (resistive measurement) vs. film thickness.

One may conclude that the RRR value at the surface is larger than in the body of the coating (estimated to about twice the overall value, i.e. 70 for 4 µm thick films). But the RRR values of the coatings deposited on the copper cavities, held at 150 or 200 °C during sputtering, may be different from those deposited on the substrates, the temperature of which is not controlled and can reach 350 °C and more. We have not yet analysed any film sputtered on a temperature controlled copper substrate.

The cavities to be sputter coated were mounted on the set-up in a class 100 laminar clean air flow. The lower part of the set-up being already under vacuum, the cavities were pumped very slowly with the turbomolecular pump through a micro - valve. It took about 15 hours to reach 10^{-4} mbar, the pressure at which the cavity's isolating valve was opened and the pumping of the cavity (with a cryopump) and bakeout of the ensemble (150 to 200°C) was started. We chose this procedure in order not to create turbulence which could carry dust inside the cavities. The residual pressure before deposition was about $5 \cdot 10^{-8}$ mbar. The magnetron cathode is moved vertically along the cavity's axis to cover all its surface. The first discharges were done in the two beam tubes, and then the cells were sputter coated. For the pentacell cavities we started with the downmost cell and finished with the uppermost one. The parameters of sputter coating are summarised in Table 1.

Table 1: Parameters for sputter coating

Cavity	number of cells	p[10^{-3} mbar]	-V [V]	I [A]	T [°C]	thickness (iris) [µm]	thickness (equator) [µm]
C1	1	4.5	390	1.5	150	5.5	3.5
C2	1	4.5	390	1.5	150	5.5	3.5
C3	1	4.5	410	1.5	150	1.8	1.6
B3	1	4.5	400	1.5	150	1.8	1.6
P1	5	4.5	390	1.5	200	1.8	1.6

3. SURFACE TEMPERATURE SCANNING IN SUPERFLUID HELIUM

3.1 Surface temperature scanning in He II

A powerful device for diagnosing superconducting accelerating cavities is the surface temperature scanning ("temperature mapping") technique. It was first applied in subcooled helium [8], for cavities at 500 MHz, and became also a tool for quantitative analysis of cavity losses [9]. The usable temperature range for subcooled helium is between 2.2 K and about 3.5 K with decreasing sensitivity towards higher temperatures. They are in first approximation sensitive to the average temperature of the interface layer between the cavity surface and the subcooled helium. The heat transfer is governed by natural turbulent convection under the buoyancy forces. At higher frequencies, however, in the before mentioned temperature range, the BCS losses become predominant, which are less interesting to be diagnosed. What is more interesting is the residual loss, which becomes visible for temperatures below 2.2 K, the lamda point of liquid helium. Therefore, temperature sensors and temperature mapping systems for measuring surface temperatures of cavities in superfluid helium (He II) have been developed [10, 11, 12]. Because of the characteristic features of superfluidity these temperature sensors must not be sensitive to the surrounding helium but to the wall temperature. This demand necessitates a very efficient thermal barrier between the sensor and He II and a very efficient thermal contact between the sensor and the cavity wall.

3.2 Temperature sensor description

For this reason a new generation of epoxy isolated scanning temperature sensors was developed at Orsay (Fig. 4).

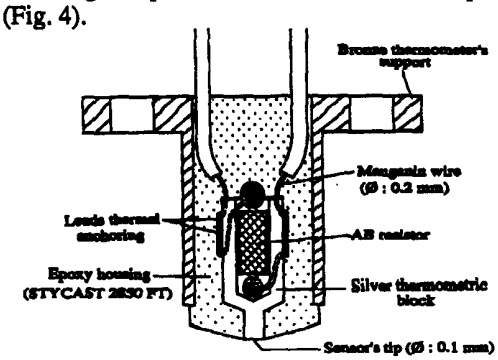

Fig. 4: Cross section of temperature sensor for superfluid helium surface temperature scan.

The main improvements of these new sensors as compared to the older generation [12] are : reduced size from 10 mm to 6 mm external diameter and consequently a higher spatial resolution, better mechanical guiding into the rotating thermometric arm, thus ensuring a better thermal contact with the cavity wall, good sensitivity (although they have a thinner insulating envelope), improved reliability.
The sensitive part is an Allen Bradley (AB) carbon resistor (100 Ω, 1/8 W) housed in a silver block with a sensor tip for thermal contact with the cavity wall. The AB resistor is glued into its housing with GE 7031 varnish or epoxy STYCAST 2850 FT. Manganin wires (Ø = 0.2 mm), thermally clamped to the silver housing over about 10 cm length, are used as electrical leads. The temperature sensor's housing is thermally insulated against superfluid helium by means of a low thermal conductivity epoxy (STYCAST 2850 FT) envelope mould around the silver block. This is altogether assembled into a mechanical support from bronze which is mounted to the rotating arm.

3.3 Calibration results

An array of 13 temperature sensors was calibrated using a special test cell and following the experimental procedure described in a previous paper [12]. Briefly, the test specimen consists of a niobium plate, resistor heated on one side and cooled by liquid helium (LHe) on the other side. The array of 13 temperature sensors to be calibrated is mounted on the LHe cooled side of the Nb specimen using Apiezon N grease as thermal bonding agent. In a first step, the temperature sensors are calibrated by comparison to a germanium sensor and the thermometric characteristic (i.e. resistance R vs. temperature T) is obtained at zero heater power. Then, the thermal response ΔT of the temperature sensors as function of the heater power P (i.e. ΔT vs. P) is measured at different bath temperature T_{bath}. In the same experiment, ΔT vs. P curves were also measured in subcooled normal helium (i.e. $T_{bath} > T_\lambda = 2.176$ K) under 1 atm bath pressure. We point out that the temperature sensor calibration tests were performed using a Nb plate specimen (RRR = 32) whereas they will be used as diagnostics on a copper surface (NbCu cavity at 1.5 GHz).
A typical temperature sensor response of the 13 temperature sensors tested simultaneously in superfluid helium at $T_{bath} = 1.52$ K and P = 388 mW heater power is ΔT = 59.6 mK with a standard deviation of 18.6 mK. The corresponding heat flux density q at the niobium - superfluid helium interface for 388 mW heater power is 30.3 mW/cm² with $H_K = 0.043 \cdot T_{bath}^{3.18} = 0.163$ W/(cm²·K) as Kapitza conductance ($T_{bath} = 1.52$ K).
The dispersion (18.6 mK) is attributed to the mechanical mounting problems of the temperature sensors on the Nb specimen resulting from differential thermal contraction between dissimilar material and deformation of the Nb plate (pressure variation from 1 atm to 4.8 mbar), and the unavoidable presence of He II microchannels inside the Apiezon N grease. As expected, the thermal response in subcooled normal helium bath at $T_{bath} = 2.5$ K is much higher (ΔT = 548 mK at P = 98 mW) with a smaller relative dispersion (σ = 18 %). But the resulting spatial resolution is lower than in superfluid helium due to a more important heat diffusion into the plate in radial direction. Moreover, the good linearity of the temperature sensors is confirmed (Fig. 5).

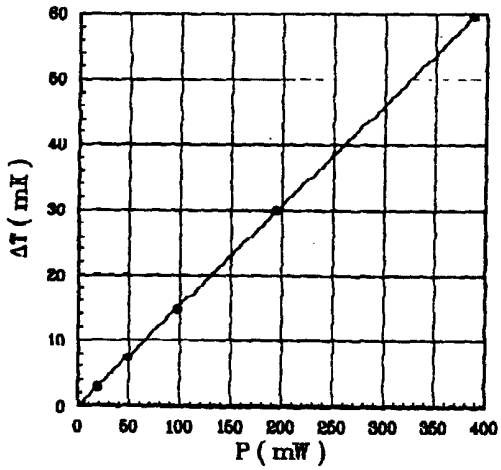

Fig. 5: Response of temperature sensor to heater power.

The effect of T_{bath} on the thermal response follows a power law (i.e. $\Delta T \propto T_{bath}^{-n}$) with an exponent n, ranging from 3.4 to 5.6. The small departure from the Kapitza exponent (i.e. $3 \leq n \leq 4$) could be attributed to the complex phenomena inside the bonding agent sandwiched between the Nb wall and the temperature sensor's tip.
A precise computation of the temperature distribution within the Nb test specimen is necessary for estimating the efficiency of the temperature sensors. A computer code POISNL developed at IPN Orsay Lab and based on finite element method was used for this purpose [14]. This code solves the non-linear steady-state heat equation with appropriate boundary conditions. The temperature sensor's efficiency, defined as the ratio of the experimental thermal response (with respect to T_{bath}) to the computed temperature jump at the Nb-HeII interface, varies from 23% for $T_{bath} = 1.9$ K up to 32 % for $T_{bath} = 1.52$ K [13]. This mean efficiency is a factor 1.5 higher [14] than previously obtained with the first epoxy temperature sensors (ø 10 mm) at $T_{bath} = 1.7$ K. Moreover, the "best" temperature sensor has a very good efficiency ($\eta = 51\%$ at $T_{bath} = 1.52$ K).

3.4 Mechanical design

To achieve good spatial resolution of the cavity surface, the resistors should be closely packed. Limitations in this sense are imposed by the diameter of the temperature sensors as well as by mechanical stability problems. The scan distance perpendicular to the equator of the cavity is 8 mm, which results in a total number of 19 temperature sensors resistors along the arm. The temperature sensor

case ("canon") is fixed with two small springs, the strength of which can be adjusted by the two screws holding them (Fig. 6). This fixation assures a continuous contact of the "canons" to the surface of the cavity. The scan distance parallel to the cavity's equator is limited by the resolution of the angle decoder of the arm.

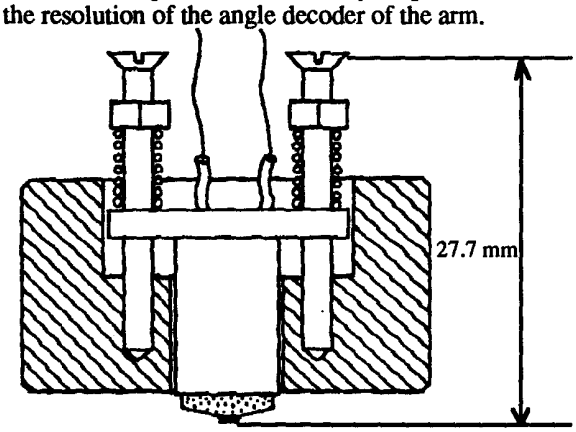

Fig. 6: Fixation of temperature sensor to scanning arm.

3.5 Data acquisition of temperature sensor signals

The resistor arm is driven by a 12 V DC electrical motor via a two gear wheel mechanism. The angle decoder is driven by the axis of the motor via a gearbox. On top of the cryostat cover light emitting diodes indicate whether the resistor arm is moving forward, backward or is in forward or backward stop position. The rotation of the arm is controlled by the computer, which in fact controls a relais card unit commuting the polarisation of the power supply for the motor. The coded angle data is received by a digital card, and read by the computer as well. The angular resolution is one degree, corresponding to a spatial resolution of 1.6 mm at the equator and 0.75 mm at the iris of the cavity. The data acquisition of the temperature sensors is based on a voltage measurement by the HP data acquisition unit "HP 3497a", which can do very fast and accurate measurements and also provides the current source. The voltage of one temperature sensor is measured in 20 ms, which simultaneously eliminates 50 Hz noise, the value is stored internally and the next channel is scanned. This technique allows to complete one scan (19 temperature sensors) in about 400 ms.

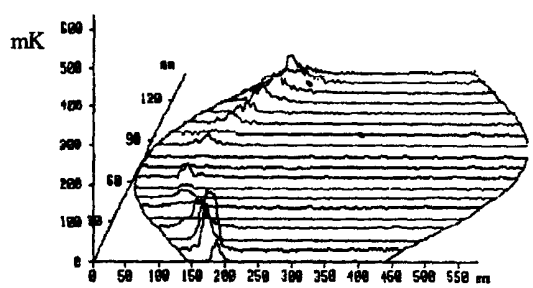

Fig. 7: Temperature map of monocell 1500 MHz NbCu cavity in He II at 6.6 MV/m, showing a signal by electron dark current.

The thermal response of the temperature sensors to a heat pulse is about 100 ms, in the same order as the response time of the cavity to RF. The signal amplitude is the difference of the surface temperature measured before the RF power is switched on and before it is switched off.
The temperature is lowered by pumping on the liquid helium bath with rotary vane pumps. The He pressure is not controlled. Therefore, during one RF pulse (1 sec), the He bath heats up. The corresponding temperature increase can reach the signal amplitude, according to the unbalance of the nominal pumping speed (400 m^3/h at 1 atm He gas pressure) and the RF power dissipated in the cavity (up to 90 W). For a quantitative analysis this contribution will be separated (by an appropriate algorithm). With 3 degrees per cycle, a complete T-map can be taken within about 10 to 60 minutes, depending on the dissipated RF power. The background signal is less than 1 mK. A typical T-map in He II, with electron dark current in the cavity taken at an accelerating gradient of 6.6 MV/m, 1.8 K, and 23 W dissipated power, is shown in Fig. 7.

4. RESULTS OF RF TESTS

The RF characteristics of the monocell cavities are published elsewhere [1], those of the pentacells are given in Table 2. The R/Q value is defined as $V^2/(2\omega U)$, with V the accelerating voltage, $\omega = 2\pi f_0$ the frequency and U the stored energy. $G = R_s \cdot Q$ is the geometry factor, and E_p/E_{acc} and B_p/E_{acc} are the ratios of the electric and magnetic peak surface fields to the accelerating gradient. The fundamental pass band frequencies are listed in Table 3. The computation was performed with the SUPERFISH code [15].

Table 2: 5-cell characteristics (computed)

R/Q	237 [Ω]
G	289 [Ω]
E_p / E_{acc}	2.8
B_p / E_{acc}	4.5 [mT / (MV/m)]
f_0	1502.877 [MHz]

Table 3: Computed and measured frequencies [MHz] of 5-cell cavity

π/5	1452.470	1449.798
2π/5	1465.811	1464.151
3π/5	1482.808	1481.570
4π/5	1497.000	1496.859
π	1502.877	1501.375

For the time being we tested 4 monocell cavities and one pentacell cavity (Table 4 and Fig. 8). The first 2 monocell cavities (C1, C2) were coated to 5 μm thickness, the next 2 (C3, B3) to 1.5 μm thickness. So was the pentacell cavity. The reason was that the niobium target was not thick enough to guarantee a larger thickness than 1.5 μm in the pentacell cavity without interruption of the discharge. Therefore, prior to the sputter coating of the pentacell cavity, these very parameters were tested in the two monocell cavities (C3 and B3).

Up till now, the RF tests were immediately performed after arrival of the cavities at CERN, i.e. no water rinsing was performed.
The cavities with a thicker layer indicate a better low field Q-value, due to a lower residual loss. In addition, their maximum accelerating gradients E_{acc} are larger, one exceeding 16 MV/m. All cavities were limited by the RF power available from a Varian 100 W TWT amplifier. All exhibited electron dark current, more pronounced in the cavities C3 and C4. None was limited by a fast quench, due to the beneficial effect of the high thermal conductivity of the copper substrate. None showed a "Q-switch" (though once a defect signal on a temperature map) or a fast decrease of Q vs. E_{acc} by excessive electron loading, thanks to the precautions taken prior and after sputter coating to avoid dust contamination. The results, which were obtained without water rinsing, are comparable to those obtained previously only after water rinsing [1].

5. CONCLUSION AND OUTLOOK

We have shown, that more rigorous application of clean work reduces the probability of "Q-switches". The level of electron loading, without rinsing, is similar to that previously obtained after high pressure water rinsing. First preliminary results of a pentacell cavity are not far from those of a monocell cavity. There are indications that cavities with a thicker coating will have a superior RF performance. Newly developed ultra sensitive temperature sensors serve as an important diagnostic tool in He II.
In the future, all cavities will be rinsed with water under low and high pressure to verify whether the RF performance can be improved.

ACKNOWLEDGEMENTS

We like to thank all people involved in the work presented here: C. Dalmas for a continuous follow up of the program, as well as A. Insomby, H. Preis, B. Thoeny, R. Jaggi, A. Lasserre, J. Benbotti, S. Forel, R. Fortin, G. Tanter, J. M. Rieubland and the cryogenic laboratory team, at CERN, and J. Martignac, J. Gobin, S. Cantacuzène at Saclay. T. G. Flynn helped us in the design and early set-up of the temperature mapping system.

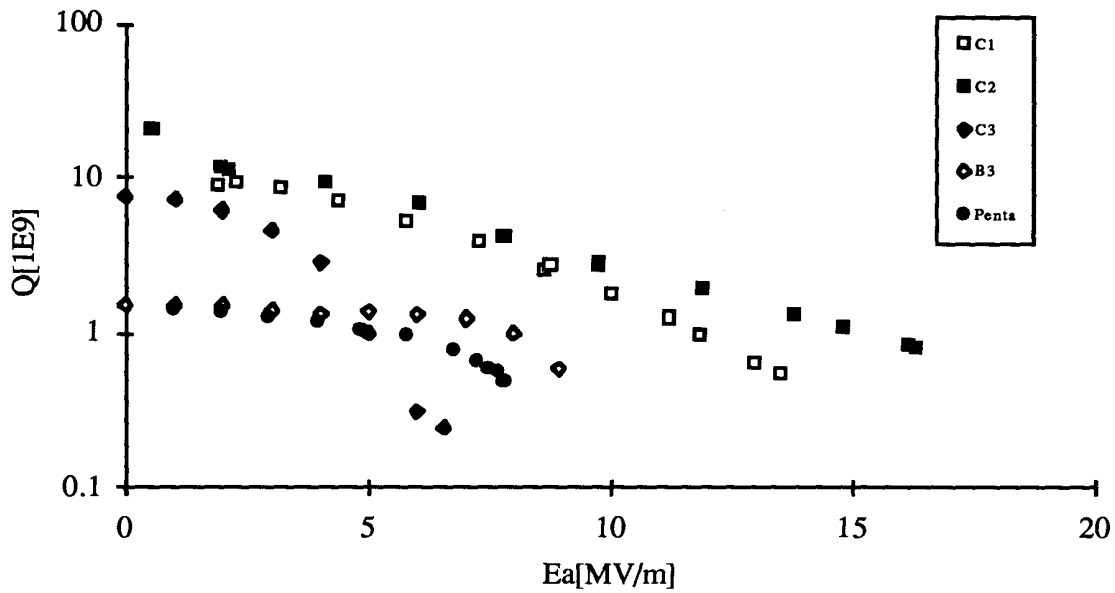

Fig. 8 : Q-values. accelerating gradient of 1500 MHz cavities (mono- and pentacell) after coating on new set-up (no water rinsing applied).

Table 4: RF test results of monocell cavities (C1, ..., B3) and 5-cell cavity (P1)

Cavity #	f [MHz]	$Q_0(E_{acc}->0)$ [10^9]	$Q(E_{acc,max})$[10^9]	$E_{acc,max}$ [MV/m]	T [K]
C1	1503.897	7.9	.54	13.6	2.2
C2	1504.249	18.4	.8	16.4	1.7
C3	1505.240	7.6	.24	6.6	1.7
B3	1500.051	1.7	.59	8.9	2.2
P1	1501.375	1.8	.49	7.9	2.2

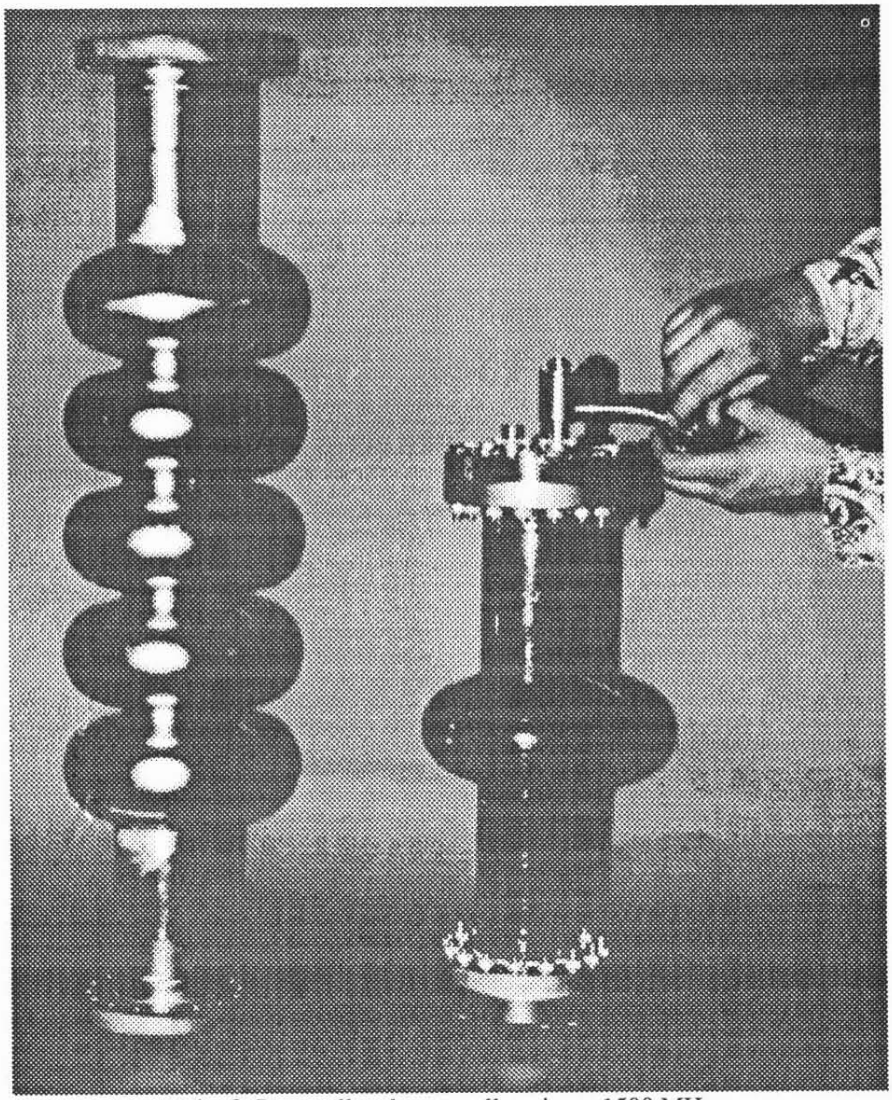

Fig. 9: Pentacell and monocell cavity at 1500 MHz.

REFERENCES

[1] Ph. Bernard et al., Proc. 5th Workshop RF Superconductivity, 12-23 August 1991, DESY, Hamburg (Germany), ed. D. Proch, 487.

[2] Ph. Bernard et al., Proc. 3rd European Part. Acc. Conf., Berlin (Germany), 24-28 March 1992, 1269.

[3] Ph. Bernard et al., this Workshop.

[4] M. Tigner, ibid. ref. 1, 1059.

[5] J. Kirchgessner, Proc. 1st Int. TESLA Workshop, July 23-26, 1990, Cornell University, Ithaca, NY (USA), CLNS-90-1029, 369.

[6] C. Hauviller, Proc. Third Int. Symp. on Plasticity and its current Applications (August 1991).

[7] C. Benvenuti et al., Proc. 20th Int. Conf. Low Temp. Physics, Eugene, Oregon, USA, 4-11 Aug 1993 and this Workshop.

[8] H. Piel and R. Romijn, CERN/EF/RF 80-3, Ph. Bernard et al., Nucl. Instr. Meth. 190 (1981) 257.

[9] R. Romijn et al., IEEE Trans. Magn. MAG-19 (1983) 1318.

[10] P. Kneisel et al., IEEE Trans. Mag. MAG-23 (1987) 1417.

[11] H. Padamsee et al., Proc. IEEE Part. Acc. Conf., vol. 3, Washington DC, USA (1987) 1824.

[12] R. Brizzi et al., Proc. ASME Heat Transfer Conf., Seattle (USA), June 1990.

[13] S. Buhler et al., this Workshop.

[14] M. Fouaidy et al., ibid. ref. 1, 547.

[15] K. Halbach and R. F. Holsinger, Part. Acc. 7 (1976) 213.